Evaluation of the Internal Particle Morphology in Catalytic Gas-Phase Olefin Polymerization Reactors

ARTICLE *in* INDUSTRIAL & ENGINEERING CHEMISTRY RESEARCH · FEBRUARY 2007

Impact Factor: 2.59 · DOI: 10.1021/ie060721s

5 AUTHORS, INCLUDING:

Vasileios Kanellopoulos
Borealis
54 PUBLICATIONS **216** CITATIONS
SEE PROFILE

Costas Kiparissides
Aristotle University of Thessaloniki
324 PUBLICATIONS **4,908** CITATIONS
SEE PROFILE

Evaluation of the Internal Particle Morphology in Catalytic Gas-Phase Olefin Polymerization Reactors

V. Kanellopoulos, E. Tsiliopoulou, G. Dompazis, V. Touloupides, and C. Kiparissides*

Department of Chemical Engineering, Aristotle University of Thessaloniki and Chemical Process Engineering Research Institute, P.O. Box 472, Thessaloniki, Greece 541 24

An unsteady-state diffusion model is developed to calculate the transport of penetrant molecules in semicrystalline nonporous polyolefin films and porous powders in terms of the internal particle morphology (i.e., pore size distribution and crystallinity) of the polymer. To calculate the diffusion coefficient of penetrant molecules in a semicrystalline nonporous polymer matrix, the free volume theory is employed. Moreover, to calculate the diffusion coefficient of penetrant species in a porous polymer matrix, a dual diffusion model, accounting for the molecular diffusion of penetrant in the pores and the amorphous polymer phase, is developed. A novel experimental setup, comprising a gravimetric magnetic suspension microbalance connected in series with an optical view cell, is employed to carry out dynamic sorption/swelling experiments of ethylene and propylene in both nonporous films and porous high-density polyethylene (HDPE) powders. Experimental sorption measurements, along with the developed unsteady-state diffusion model, are then employed to calculate the diffusion coefficient of α-olefins in porous and nonporous semicrystalline HDPE as well as the overall porosity of HDPE powders. Finally, to reconstruct the pore size distribution in a porous polyolefin particle in terms of the estimated overall particle porosity and the size distribution of the microparticles, a diffusion-limited aggregation (DLA) model is developed. It is shown that the morphological characteristics of porous polyolefin particles (i.e., porosity and pore size distribution) can be described using the proposed DLA model in terms of the size distribution of the microparticles and the extent of microparticles fusion.

Introduction

The internal morphology of the polymer particles produced in catalytic olefin polymerization reactors is a fairly complex function of the catalyst type (e.g., Ziegler−Natta (Z−N), Philips chromium, metallocenes, etc.), the catalyst prepolymerization conditions, the process type (e.g., slurry, gas phase), and the reactor operating conditions (e.g., temperature, monomer/comonomer ratio, etc.). In general, the monomer mass-transfer rate from the bulk phase to the dispersed catalyst active sites in a growing polymer particle will depend on the internal particle morphology (e.g., micro- and macroporosity) as well as the mass fraction of the crystalline polymer phase.[1−3] Moreover, it is well-established that in catalytic olefin polymerization the internal particle morphology can significantly change during polymerization. Thus, the evolution of the internal particle morphology is one of the most important research issues in the polyolefin industry today for it can have a strong impact on the transport properties of the monomer(s) and, thus, on the polymerization rate and polymer molecular properties.

The solid, catalyzed, gas-phase polyolefin production usually takes place in continuous fluidized bed reactors (FBR). In this process, prepolymerized catalyst particles in the size range of 20−80 μm or polymer particles (e.g., 50−300 μm) produced in an upstream reactor unit of a multistage process are continuously fed into the FBR at a point above the gas distributor and react with the incoming fluidizing gas mixture of monomer(s) to form a broad distribution of polymer particles (e.g., 100−5000 μm). At the very early stage of polymerization, the polymer formed inside the catalyst pores causes catalyst fragmentation and the formation of a large number of microparticles. As the polymerization proceeds, the catalyst microparticles are encapsulated by the growing polymer phase, while at the same time, the porosity of the particles decreases.

In the open literature, a great number of publications have been appeared dealing with the mathematical modeling of the growth of a single polymer particle in heterogeneous catalytic olefin polymerizations.[1−5] Among the various single-particle growth models, the multigrain model (MGM)[2,6] and the polymeric flow model (PFM)[1,7] are considered to be the closest approximations of the actual physical and chemical phenomena taking place in a polymer particle. Both models can provide estimates of the overall particle polymerization rate and spatial distribution of temperature, monomer(s), and polymer molecular properties via the solution of a system of partial differential equations, describing the conservation of energy and various molecular species in a growing polymer particle. The PFM offers the advantage of a relatively simple mathematical formulation via the hypothesis of the pseudohomogeneous reaction medium that greatly facilitates the numerical solution of the resulting moving boundary value problem. On the other hand, the MGM incorporates a more detailed picture of the diffusion phenomena occurring at both micro- and macroparticle levels that considerably increases its mathematical complexity and, thus, the computational effort. However, knowledge of the size and radial position of the microparticles in a growing polymer particle can be a useful means for the determination of the internal particle morphology. In fact, the works of Debling and Ray[6] and Hamba et al.[8] clearly show that the MGM can be employed to model the variation of the internal particle morphology during polymerization.

Chiovetta[9] and Laurence and Chiovetta[10] employed a MGM to evaluate the internal particle morphology in a gas-phase Z−N ethylene polymerization. The macroparticle was assumed to consist of several concentric layers of microparticles, and the governing system of mass and energy balances was solved at both levels of particle morphology (i.e., micro and macro). They

* To whom correspondence should be addressed. Tel.: + 30 2310 99 6211. Fax: +30 2310 99 6198. E-mail: cypress@cperi.certh.gr.

10.1021/ie060721s CCC: $37.00
Published on Web 02/22/2007

presented different relationships to estimate the number of microparticles per layer as a function of the assumed packing geometry, and the microparticle and macroparticle dimensions. Estenoz and Chiovetta[11,12] developed a model to calculate the microparticle fragment size from experimental pore size distribution measurements.[13,14] They found that the porosity of the nonfragmented particle was lower than that of the fragmented one (e.g., 0.3 vs 0.42). Moreover, they reported that the monomer diffusivity in the nonfragmented macroparticle was 100 times smaller than that of the fragmented one.

Hutchinson et al.[2] developed a single-particle growth model that accounted for the variation of the porosity with respect to the particle radius. They showed that the porosity can be a function of radial position, and thus, the local particle growth rate can depend on the particle radius. Galli and Haylock,[15] Simonazzi et al.,[16] and Galli[17,18] pointed out the critical role of particle morphology on the high-impact polypropylene (hi-PP) and specialty multilayered binary and ternary copolymers produced in multistage reactor configurations. Pater et al.[19] experimentally investigated the effect of polymerization temperature on the morphology of polypropylene (PP) produced in liquid propylene in the presence of a Z−N catalyst. They showed that, in the case of a non-prepolymerized catalyst at high polymerization temperatures, the PP exhibited a spongelike morphology. On the other hand, when a prepolymerized catalyst was employed, the particle morphology was independent of the polymerization temperature. They indicated that there is a need for the development of comprehensive mathematical models to explain the experimental observations on the evolution of particle morphology for highly active catalysts. Agarwal[20] developed a single-particle model to investigate the effect of the deformability of the polymer chains on the internal particle morphology and monomer transfer rate. It was concluded that the polymer particle morphology is a complex function of the morphology of original catalyst support, friability of the support material, polymer type, and polymerization conditions.

In view of all the above theoretical and experimental observations, a fresh look at the evaluation of internal particle morphology (i.e., overall porosity and pore size distribution) in catalytic olefin polymerizations is highly desirable. In the present study, an unsteady-state diffusion model is first developed to calculate the transport of penetrant(s) molecules in semicrystalline, high-density polyethylene (HDPE), nonporous films, and porous powders in terms of the internal particle morphology (i.e., pore size distribution and crystallinity) of the polymer. To estimate the overall particle porosity dynamic sorption measurements of α-olefins (i.e., ethylene, propylene) in HDPE, nonporous films and porous powders are employed, along with the developed unsteady-state diffusion model. Finally, a diffusion-limited aggregation (DLA) model is employed to reconstruct the pore size distribution in a porous polyolefin particle in terms of the estimated overall particle porosity and the size distribution of the microparticles.

Diffusion of α-Olefins in Semicrystalline Polymer Films and Powders

To predict the transport of low molecular weight α-olefins in semicrystalline polymer films and powders, an unsteady-state diffusion model was employed. The model takes into account the effect of polymer-induced convection at the moving boundary condition.

Let us assume that a nonporous polymer film of initial thickness L_{0x} (see Figure 1) is exposed at time $t = 0$ to a gaseous α-olefin atmosphere. Assuming that, at the solid−gas interface,

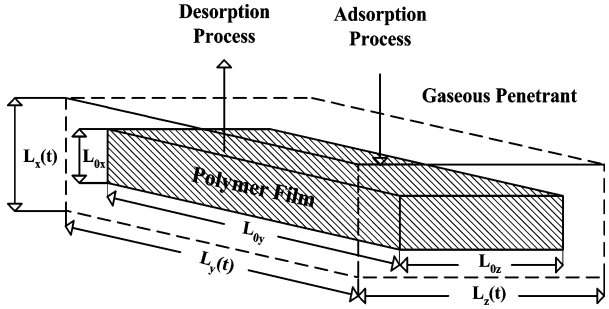

Figure 1. Simultaneous diffusion and swelling in a nonporous polymer film.

the penetrant concentration in the film is at equilibrium (i.e., $C_i(t,L_x) = C_{i,\mathrm{eq}}$), one can derive the following unsteady-state mass balance equation accounting for the diffusion of the penetrant molecules in the polymer film (see Figure 1).

$$\frac{\partial C_i}{\partial t} + \frac{\partial (uC_i)}{\partial x} = \frac{\partial}{\partial x}\left(D_i^{\mathrm{p}} \frac{\partial C_i}{\partial x}\right) \tag{1}$$

initial condition

$$C_i(x,0) = 0 \quad \text{at} \quad t = 0 \tag{2}$$

boundary conditions

$$\partial C_i/\partial x = 0 \quad \text{at} \quad x = 0 \tag{3}$$

$$C_i(t,L_x(t)) = C_{i,\mathrm{eq}} \quad \text{at} \quad x = L_x(t) \tag{4}$$

where D_i^{p}, C_i, and $C_{i,\mathrm{eq}}$ are the diffusion coefficient and the concentrations of the i penentrant species at time t and at equilibrium, respectively. It should be pointed out that the variation of the film thickness, $L_x(t)$, due to polymer swelling and, thus, the velocity at the moving boundary, $u(t)|_{x=L_x(t)} \cong L_x(t) \cong (\mathrm{d}L_x(t)/\mathrm{d}t)$, were measured experimentally by monitoring the volume change of the polymer film via an optical apparatus (see Experimental Measurements). Assuming that the partial specific volumes of the two species (i.e., penetrant and polymer) are constant, then the local average velocity, u, will be equal to zero, and therefore, the convective term in eq 1 can be eliminated (i.e., $\partial(uC_i)/\partial x = 0$).

The inclusion of the moving boundary condition (see eq 4) greatly complicates the numerical solution of eq 1. Thus, to avoid the solution of the original moving boundary value problem, a dimensionless space variable $z(t) = x/L_x(t)$ and a dimensionless concentration (i.e., $Y_i(t,z) = C_i(t,x)/C_{i,\mathrm{eq}}$) are defined. The new spatial variable allows the transformation of the time-dependent boundary condition, eq 4, into a time invariant one, $z \in [0, 1]$. Accordingly, the spatial and the time derivatives ($\partial Y_i/\partial x$) and ($\partial Y_i/\partial t$) of the dimensionless concentration are expressed in terms of the new variable z:

$$\left(\frac{\partial Y_i}{\partial x}\right) = \left(\frac{\partial Y_i}{\partial z}\frac{\partial z}{\partial x}\right) = \left(\frac{1}{L_x}\frac{\partial Y_i}{\partial z}\right) \tag{5}$$

$$\left(\frac{\partial Y_i}{\partial t}\right) = \left(\frac{\partial Y_i}{\partial t}\right) + \left(\frac{\partial Y_i}{\partial z}\frac{\partial z}{\partial t}\right) = \frac{\partial Y_i}{\partial t} - \frac{x\dot{L}_x}{L_x^{\,2}}\frac{\partial Y_i}{\partial z} \tag{6}$$

Using the above definitions, the original moving boundary value problem (eqs 1−4) can be recast into the following fixed boundary one:

continuity equation (planar coordinates)

$$\frac{\partial Y_i}{\partial t} - \frac{1}{L_x^2}\left[L_x \dot{L}_x z + \frac{\partial D_i^p}{\partial z}\right]\frac{\partial Y_i}{\partial z} = \frac{D_i^p}{L_x^2}\frac{\partial^2 Y_i}{\partial z^2} \quad (7)$$

initial condition

$$Y_i = 0 \quad \text{at} \quad t = 0 \quad (8)$$

boundary conditions

$$\partial Y_i/\partial z = 0 \quad \text{at} \quad z = 0 \quad (9)$$

$$Y_i = 1 \quad \text{at} \quad z = 1 \quad (10)$$

Similarly, the unsteady-state diffusion of penetrant molecules in a spherical polymer particle can be described by the following continuity equation:

continuity equation (spherical coordinates)

$$\frac{\partial Y_i}{\partial t} - \frac{1}{R^2}\left[R\dot{R}z + \frac{2D_i}{z} + \frac{\partial D_i}{\partial z}\right]\frac{\partial Y_i}{\partial z} = \frac{D_i}{R^2}\frac{\partial^2 Y_i}{\partial z^2} \quad (11)$$

initial condition

$$Y_i = 0 \quad \text{at} \quad t = 0 \quad (12)$$

boundary conditions

$$\partial Y_i/\partial z = 0 \quad \text{at} \quad z = 0 \quad (13)$$

$$Y_i = 1 \quad \text{at} \quad z = 1 \quad (14)$$

where $R(t)$ is the varying particle radius due to polymer swelling, $\dot{R}(t) \cong (dR(t)/dt)$ is the velocity at the moving boundary, and $z = (r/R(t))$ is a dimensionless radius.

Both diffusion models consist of a stiff nonlinear partial differential equation (eq 7 or 11) and a number of initial and boundary conditions (eqs 8−10 or 12−14). In both cases, the partial differential equations were solved by the global collocation method. Specifically, the partial differential equation was first discretized with respect to the planar or the radial coordinate, or both, at selected collocation points, while the unknown variable was approximated by a Lagrange interpolation polynomial.[21] The resulting differential equations were then integrated using the Petzold−Gear method. It can easily be shown that the mass of the sorbed species at time t, $M_i(t)$, will be given by the following integral:

$$M_i(t) = M_{i,eq}\int_0^1 Y_i(z)\,dz \quad (15)$$

where $M_{i,eq}$ is the total mass of the sorbed species i at equilibrium.

Calculation of the Penetrant Diffusion Coefficient in Nonporous Polymer Films. To calculate the diffusion coefficient of the penetrant molecules, D_i^p, in a semicrystalline, nonporous polymer matrix, the free volume theory was employed.[22,23] Thus, following the original developments of Vrentas and Duda,[24] the diffusion coefficient of α-olefins in a semicrystalline, nonporous polyolefin (e.g., film, powder) was expressed as follows:

$$D_i^p = D_{0,i}^p \exp(-\gamma_i(\omega_i V_i^* + \omega_p V_p^* \xi_{ip})/V_{FH})\tau^{-1} \quad (16)$$

where the subscripts i and p refer to the penetrant molecules and the polymer, respectively. $D_{0,i}^p$ is a pre-exponential constant and γ_i is an overlap factor (taking values in the range of 0.5−1), accounting for the amount of free volume shared between different penetrant molecules. ω_i and ω_p are the weight fractions of the penetrant molecules and polymer, respectively. V_i^* denotes the specific critical hole free volume of the i sorbed species, required for their displacement. Note that the value of V_i^* can be estimated using the group contribution method of Haward and the chemical composition of the penetrant molecules.[23] The parameter ξ_{ip} is defined by the ratio of V_i^* over the specific critical hole free volume of the jumping unit of the polymer chains, V_{pk}.[23] V_{FH} is the overall free volume of the system given by the weighted sum of the corresponding free volumes of the penetrant molecules and the amorphous polymer chains.[23] Finally, the parameter τ accounts for the fact that the penetrant molecules must follow a longer pathway than the actual thickness of the film or particle radius to circumvent the dispersed polymer crystalline domains. This is conveniently described by a single factor, the so-called geometrical impedance factor τ, defined by the ratio of the diffusivity of the penetrant molecules in a completely amorphous polymer to that corresponding to a semicrystalline one. Equation 16 refers to the local diffusion coefficient, $D_i^p(x)$. Accordingly, the overall (effective) diffusion coefficient, $D_{i,eff}^p$, in the polymer film can be calculated by integrating the local diffusion coefficient, $D_i^p(x)$, with respect to the polymer film's thickness, L_x:

$$D_{i,eff}^p = \int_{L_x} D_i^p(x)\,dx / \int_{L_x} dx \quad (17)$$

Calculation of the Penetrant Diffusion Coefficient in Porous Polymer Particles. The diffusion of the penetrant species from the bulk gas phase to the amorphous polymer phase in a spherical, porous, semicrystalline polymer particle is assumed to occur via a dual mechanism that comprises molecular diffusion of the penetrant species through the particle's pores and the amorphous polymer phase (see Figure 2).

According to the general gas diffusion theory of Chapman−Enskog, the diffusion coefficient of species i in the pores of size $d_p \geq 0.02$ μm will be given by the following equation:[25−27]

$$D_i^0 = 1.86 \times 10^{-3} T^{3/2} (MW_i)^{-1/2}/(P\sigma_i^2 \Omega) \quad (18)$$

where P, MW_i, and σ_i are the pressure, the molecular weight, and the collision diameter of the penentrant molecules, respectively. The dimensionless quantity Ω is a complex function of Leonard-Jones 12-6 potential, temperature, and energy of interaction between the like penetrant molecules.

As mentioned above, diffusion of the penetrant molecules also takes place through the amorphous polymer phase. In this case, the diffusion coefficient of the penetrant species will depend on the temperature, the concentration of sorbed species, and the degree of polymer crystallinity (see eq 16).

In the present study, the random pore model of Wacao and Smith was employed to take into account the dual mode of penetrant transport from the bulk gas-phase to the polymer phase.[28−30] A schematic representation of the random pore model is illustrated in Figure 2. As can be seen, one can identify three possible transport paths for the diffusion of the penetrant species through two hypothetical consecutive polymer layers: (i) molecular diffusion through the open pores, (ii) molecular diffusion through the amorphous polymer domains, and (iii) combined molecular diffusion through the open pores of one layer and the amorphous polymer phase of the next (and vice versa).

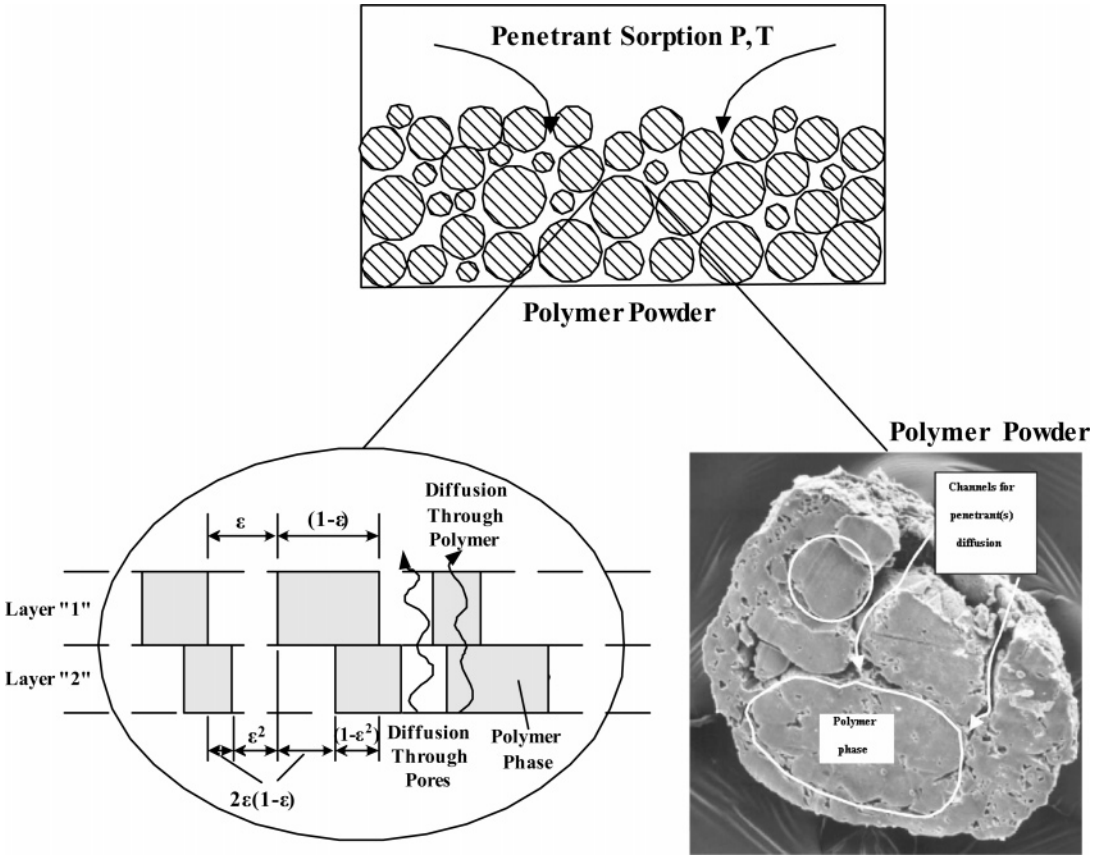

Figure 2. Dual diffusion mechanism in a porous polymer particle.

It is apparent that the selected arrangement of the pores in the random pore model of Wacao and Smith (see Figure 2) does not represent the real pore geometry in a polymer particle. Furthermore, the pores are not parallel to the direction of diffusion. Thus, a tortuosity factor τ_f, is often introduced to take into account the tortuous nature of the pores and the presence of random constrictions in the pore geometry. Based on the above random pore configuration and model assumptions, it can be shown that the overall diffusion coefficient, $D_{i,\text{eff}}$, of the penetrant molecules in a semicrystalline, porous polymer particle can be expressed as follows:[30]

$$D_{i,\text{eff}} = \frac{\epsilon}{\tau_f^2} D_i^0 + (1-\epsilon)(1+3\epsilon) D_{i,\text{eff}}^p \qquad (19)$$

where $D_{i,\text{eff}}^p$ is the diffusion coefficient of the penetrant species i in the amorphous polymer phase given by eq 17. It should be pointed out that the first term on the right-hand side of eq 19 accounts for the penetrant mass transfer via the particle's pores while the second term accounts for the penetrant transport through the amorphous polymer phase. As will be explained later, in Experimental Measurements, the overall particle porosity, ϵ, can be estimated by fitting the unsteady-state diffusion model (eqs 11−19) to dynamic experimental sorption measurements of α-olefins in porous polyolefin particles.

Reconstruction of the Internal Particle Morphology

In the heterogeneous catalytic olefin polymerization, the evolution of the internal particle morphology involves the growth and aggregation of a great number of microparticles to form latger particle aggregates that can be further fused or extruded. In general, the internal polymer particle morphology will be the outcome of a series of chemical and physical processes, including catalyst fragmentation, microparticle growth, aggregation, and fusion.

Diffusion-Limited Aggregation Model. As has been reported by many investigators, the polymer particles can exhibit a rough internal structure with tortuous pore channels that follows a fractal geometry.[14,15,20,31,32] Moreover, it has been experimentally shown that the concentration of microparticles near the macroparticle perimeter can be higher than that in the center of the growing polymer particle.[9−14] As a result, large open structures can be formed in the center of the macroparicle.

The formation of a fractal structure due to particle growth and aggregation processes has been studied for a number of systems in nature.[33] In the present study, in order to model the microparticle aggregation−fusion processes inside a polymer macroparticle under certain polymerization conditions (e.g., temperature, microparticle size, particle diameter, etc.), the macroparticle was initially divided into a number of concentric shells (i.e., layers). Furthermore, it was assumed that the microparticle formation and aggregation (fusion) probabilities could vary from one shell to another.[34−36]

According to the proposed DLA model, a microparticle is first formed inside a shell and then diffuses until it sticks either to a network of existing microparticles or arrives at the shell's perimeter. It was found that the number of initial growth centers in a shell as well as the length of the microparticle diffusion step did not influence significantly the final value of the calculated porosity. On the other hand, the total number and the size distribution of the microparticles affected the final porosity value. In general, large microparticles are more restricted in their movements and produce more loosely packed structures. In the present study, it was assumed that the microparticles followed a log-normal distribution. To simplify the numerical calculations, a two-dimensional DLA model was

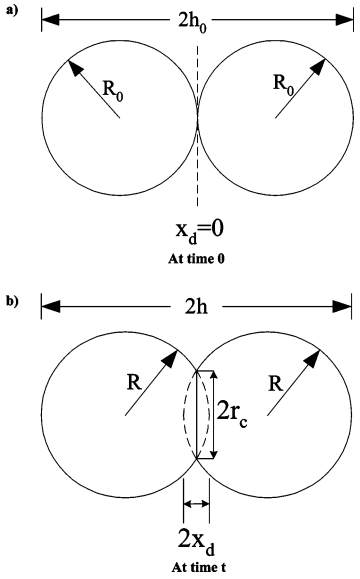

Figure 3. Schematic representation of the microparticle fusion precess.

employed. Thus, to estimate the actual 3-D particle porosity from the 2-D results, the following equation was applied:[33]

$$\epsilon_{vol} = (\epsilon_{surf})^{((\text{fractal dimension} + 1)/\text{fractal dimension})} \qquad (20)$$

In summary, the proposed DLA model included the following parameters: (i) the number of selected shells in a polymer macroparticle. Note that the individual shells can be characterized by different microparticle formation and aggregation (fusion) probabilities (0−1). (ii) The number of microparticle formation centers in a shell. (iii) The total number of microparticles. (iv) The mean diameter and standard deviation of the log-normal microparticle size distribution. (v) The diffusion length that a microparticle can travel in a single step (e.g., usually 1 or 2 times the microparticle radius). (vi) The fusion factor. This parameter characterizes the extent of microparticle fusion and can vary from 0 to 1).

Calculation of the Extent of Microparticle Fusion. The extent of microparticle fusion usually increases with temperature that reduces the final particle porosity. In general, any physically meaningful model should predict an increase in the extent of microparticle fusion with increasing temperature, with increasing polymer interfacial forces, and with decreasing polymer melt viscosity.

In the present study, a two-microparticle fusion model was employed to calculate the extent of particle fusion (i.e., fusion factor) in terms of the rheological polymer properties, microparticle radii, and temperature. According to the proposed model (see Figure 3), the extent of microparticle fusion is expressed in terms of the radius of the contact circle, r_c, or the center to center distance, $2h$, of the two fused microparticles (see Figure 3b). Note that the microparticles are drawn together under the influence of interfacial tension forces acting on the contact line of radius r_c. It should be noted that the two polymer microparticles are "fused together" if the radius of the contact circle exceeds a certain value (i.e., $r_c \geq r_{c,max}$) or the center-to-center particle distance satisfies the condition $2h \leq 2h_{min}$. Under these conditions, a viscoelastic polymer flow can be established between the two microparticles, resulting in a successful particle fusion event.

It is well-known that the polymer rheological behavior can be described in terms of a viscoelastic model combining the viscous and elastic responses of the material to an applied load.

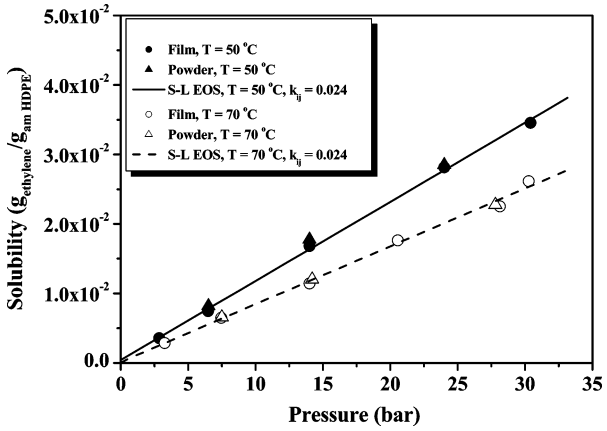

Figure 4. Solubility of ethylene in HDPE at different temperatures and pressures.

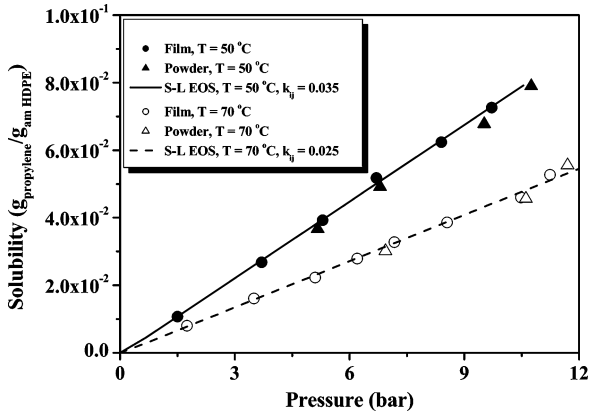

Figure 5. Solubility of propylene in HDPE at different temperatures and pressures.

A polymer that exhibits varying degrees of these combined responses is called viscoelastic material. In general, the viscoelastic behavior of a polymer can be described by a number of springs and dashpots, with temporary connections representing entanglements or forces. The simplest viscoelastic model, describing the elastic and viscous characteristics of a polymer, is the Maxwell model that combines the Hookean equation for solids (i.e., $\sigma_e = -Gl_e$) and the Newtonian equation for liquids (i.e., $\sigma_v = \mu\dot{l}_v$). In this study, the Maxwell model, in which the spring (elastic part) and the dashpot (viscous part) are arranged in series, was employed to describe the viscoelastic polymer flow between the two fused polymer microparticles.

Assuming that a squeezing polymer flow is established between the two microparticles, the well-known Stefan−Maxwell equation can be employed to describe the time-depedent polymer deformation under an applied load, F_{ve}:[37]

$$\lambda_o \frac{dF_{ve}}{dt} + F_{ve} = -\frac{3\pi}{8}\frac{\mu r_c^4 \dot{h}}{h^3} + \frac{2\lambda_o \dot{r}_c F_{ve}}{r_c} \qquad (21)$$

where h is the center-to-center distance between the two fused microparticles, $\lambda_o = \mu/G$ is the characteristic relaxation time for a Maxwell fluid, G is the Young's elasticity modulus, μ is the apparent polymer viscosity, and r is the radius of the contact circle (see Figure 3).

The viscoelastic force, F_{ve}, acting on the contact circle of the two microparticles will be given by the Laplace−Young equation:

$$F_{ve} = \gamma_s \pi r_c^2 \qquad (22)$$

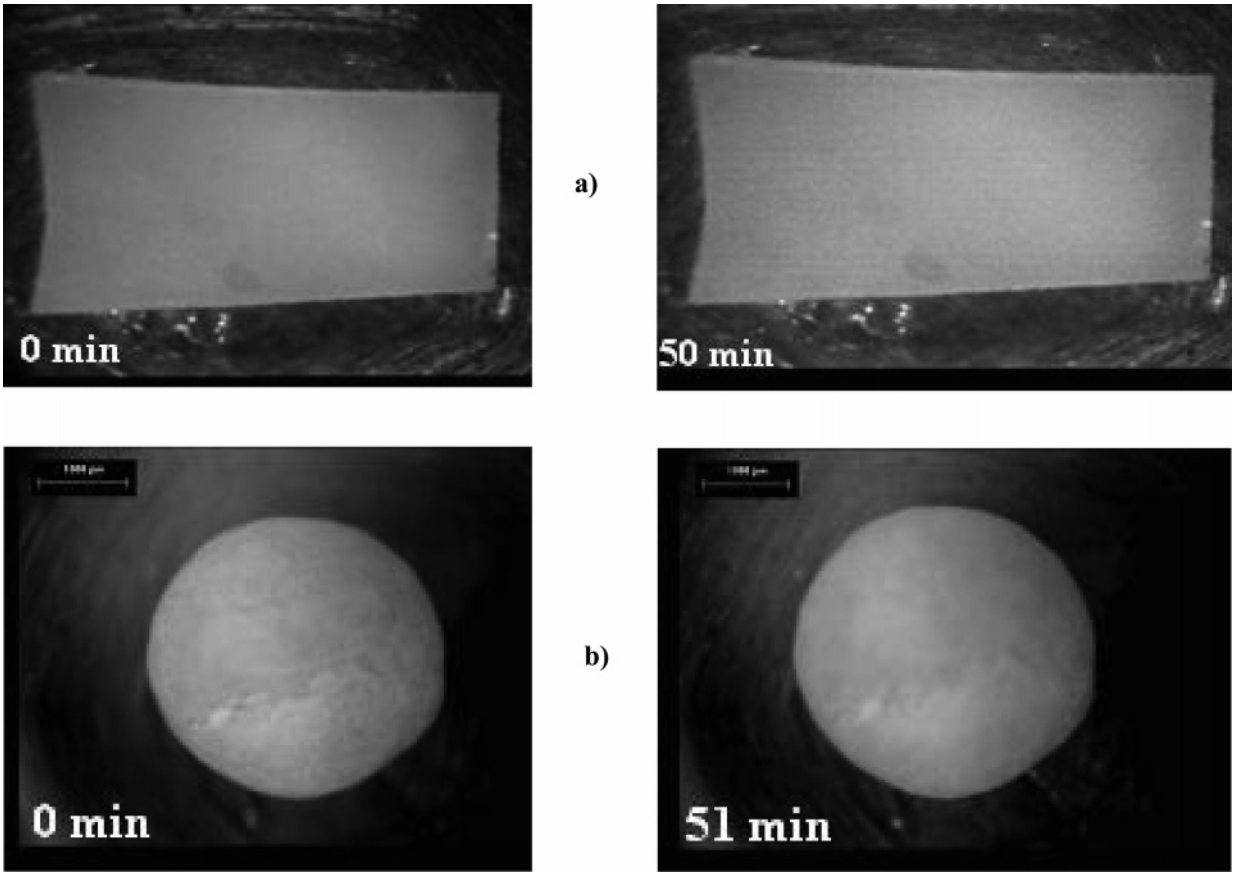

Figure 6. Time evolution of swelling of polymer films and particles.

where γ_s is the polymer−polymer interfacial tension (in kg/s^2). It can be easily shown, based on mass conservation and geometric arguments, that, for two equal-size particles, the displacement distance, x_d, the contact (fusion) radius, r_c, and the variation of the microparticle radius, R, will be given by the following equations (see Figure 3):

$$r_c^2 = (2R - x_d)x_d \tag{23}$$

$$R^3 = R_0^3 + (2R + h)(R - h)^2/4; \quad h = R - x_d \tag{24}$$

where R_0 is the microparticle radius at time zero.

From the numerical solution of eqs 21−24, one can calculate the variation of x_d, R, and r_c with time. A differential-algebraic equation solver (i.e., DDASPG from IMSL) was employed for the numerical integration of the resulting model equations. Subsequently, the fusion factor was calculated by the ratio (r_c/R) or/and(h/h_0).

Experimental Measurements

Sorption Measurements. A new experimental setup was built to carry out dynamic sorption measurements of α-olefins in polymer films and powders. The experimental system comprised a gravimetric magnetic suspension microbalance (i.e., Rubotherm, MSB) for the determination of mass of sorbed species by the solid polymer sample. The microbalance was connected in series with an optical view cell (VC) for the on-line measurement of the degree of polymer swelling. A high-resolution camera attached to a stereomicroscope was employed for continuous frame grabbing and, thus, the determination of the change in volume of the sample due to polymer swelling. The dynamic sorption measurements in either polymer films or powders were carried out under isothermal and isobaric conditions. Porous HDPE particles of an approximate diameter of 0.035 cm (kindly supplied by Borealis) were employed for the preparation of nonporous HDPE films of an approximate thickness of 0.040 cm. The films were prepared with the aid of a hot-press apparatus by melting and pressing the HDPE grains/particles at a temperature of ∼130 °C for 15 min. The mass fraction of crystalline polymer phase, ω_c, was measured with a differential scanning calorimeter. Specifically, by measuring the heat of fusion of the polymer sample (i.e., film and powder) and dividing it by the heat of fusion of 100% crystalline polymer (e.g., 270.3 kJ/kg), the value of ω_c could be determined.[38] From the measured values of ω_c and the densities of crystalline (ρ_c = 0.997g/cm^3) and amorphous (ρ_{am} = 0.854 g/cm^3) polymer, the density of the semicrystalline polymer (ρ) could be deduced:[38]

$$\omega_c = \frac{\rho_c}{\rho}\left(\frac{\rho - \rho_{am}}{\rho_c - \rho_{am}}\right) \tag{25}$$

In Figures 4 and 5, the experimentally measured solubilities of ethylene and propylene in HDPE films and powders are compared with model predictions obtained by the Sanchez−Lacombe (S−L) equation of state (S−L EOS), at different pressures and temperatures. It is important to point out that in all theoretical calculations the characteristic parameter values T^*, P^*, and ρ^* used in the S−L EOS were directly obtained from molecular dynamic simulations.[39] Note that the value of the binary interaction parameter, k_{ij}, in the S−L EOS, for the ethylene/HDPE system was kept constant (i.e., independent of temperature). On the other hand, the value of the interaction

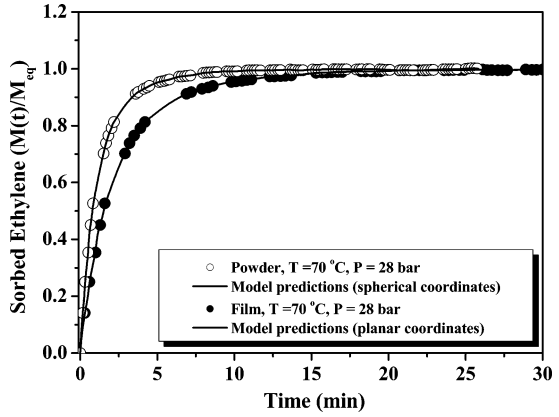

Figure 7. Measured and predicted sorption curves in a polymer film and a powder for the ethylene−HDPE system (T = 70 °C, P = 28.0 bar).

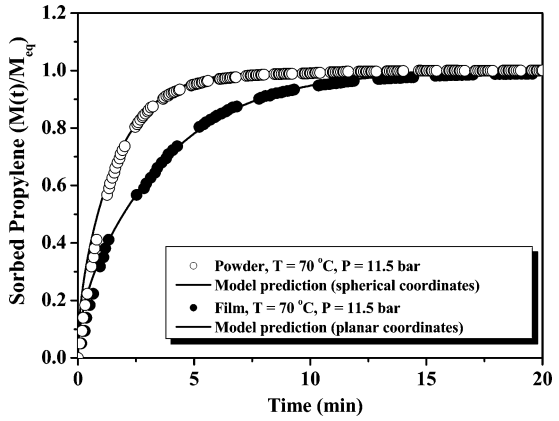

Figure 8. Measured and predicted sorption curves in a polymer film and a powder for the propylene−HDPE system (T = 70 °C, P = 11.5 bar).

parameter, k_{ij}, for the propylene/PE binary system was found to decrease with temperature.[39]

Swelling Measurements. Due to the penetrant mass uptake by the amorphous polymer phase, the volume of the polymer sample increases during a dynamic sorption experiment. In the present study, the degree of polymer swelling due to the dissolution of penetrant molecules in the polymer phase was determined by measuring the change in volume of the polymer film or powder placed in the view cell, operated in series with the microbalance. Specifically, a polymer sample of known dimensions (i.e., length and width or radius) was initially placed inside the view cell. Accordingly, the cell was sealed and heated to a desired temperature while the gas pressure was increased to a specified value. The change in the sample's dimensions were measured on-line using a video camera filming through the optical window of the cell. This allowed the real-time visualization of the swelling process. Figure 6, shows some optical images of the swollen polymer films and particles obtained by a high-resolution camera at different times. The optically obtained size measurements were then fitted to the following equations, describing the time variation of the characteristic dimensions of the polymer films and powders:

$$L_k(t) = L_{0k}(1 + \alpha(1 - e^{-bt})); \quad k = x,y,z \quad \text{(polymer film)} \tag{26}$$

$$R(t) = R_0(1 + c(1 - e^{-dt})); \quad \text{(polymer particle)} \tag{27}$$

Using the above polymer swelling equations, the dynamic sorption measurements (i.e., obtained by the Rubotherm microbalance) were properly corrected by applying the following equation:

$$M_{i,\text{corr}}(t) = M_{i,\text{meas}}(t) + \Delta V(t)\rho \tag{28}$$

where $M_{i,\text{corr}}(t)$, $M_{i,\text{meas}}(t)$, $\Delta V(t)$, and ρ denote the corrected total mass of the sorbed species at time t, the measured mass of the penetrant species at time t, the measured volume increase due to polymer swelling, and the density of the penetrant species, respectively.

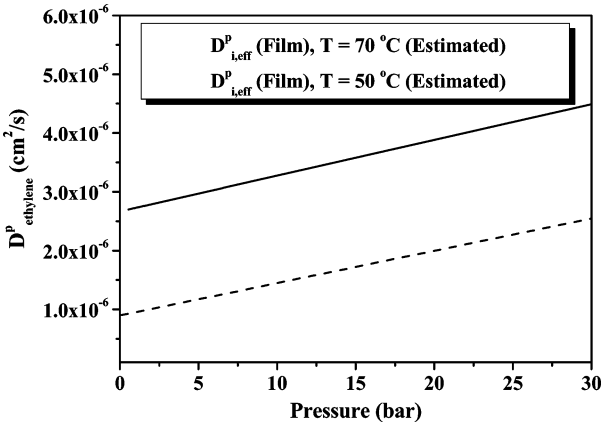

Figure 9. Estimated values of ethylene diffusion coefficient, $D^{p}_{i,\text{eff}}$, in HDPE films at different pressures and temperatures.

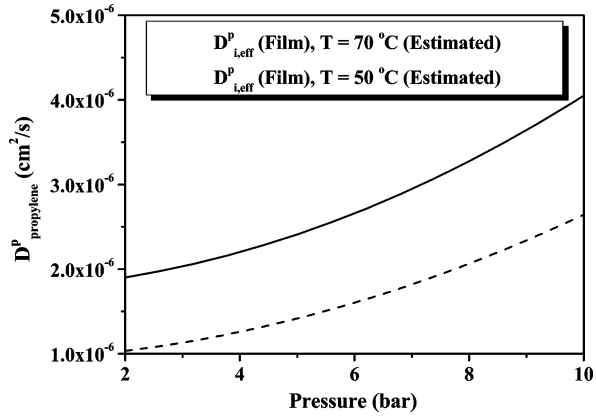

Figure 10. Estimated values of propylene diffusion coefficient, $D^{p}_{i,\text{eff}}$, in HDPE films at different pressures and temperatures.

Table 1. Numerical Values of the Physical and Transport Parameters Used in the Theoretical Calculations

parameters	poly-ethylene	ethylene	propylene
$D^{p}_{0,i}$ (cm²/s) (at T = 50 °C)		0.31	2.7
$D^{p}_{0,i}$ (cm²/s) (at T = 70 °C)		0.46	2.9
$D^{p}_{0,i}$ (cm²/s) (reported in the literature)[40−43]		0.26−0.65	1.3−3.5
V^{*}_{i} (cm³/g)[23]	1.32	1.32	1.23
γ_i[23]	-	0.75	0.75
ω_c	0.44		
ρ_{am} (kg/m³)[38]	0.854		
ρ_c (kg/m³)[38]	0.997		
τ[22]	1.30		
τ_f[28]	10		
γ_s (kg/s²) (at T = 50 °C)[45]	0.031		
γ_s (kg/s²) (at T = 70 °C)[45]	0.030		
G (kg m^{-1} s^{-2}) (at T = 70 °C)[45]	2.1×10^8		
μ (kg/m/s) (at T = 50 °C)[45]	1.15×10^6		
μ (kg/m/s) (at T = 70 °C)[45]	0.82×10^6		

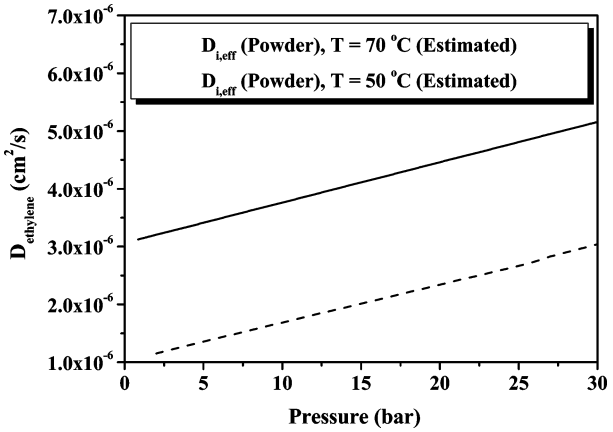

Figure 11. Estimated values of ethylene diffusion coefficient, $D_{i,\mathrm{eff}}$, in HDPE powders at different pressures and temperatures.

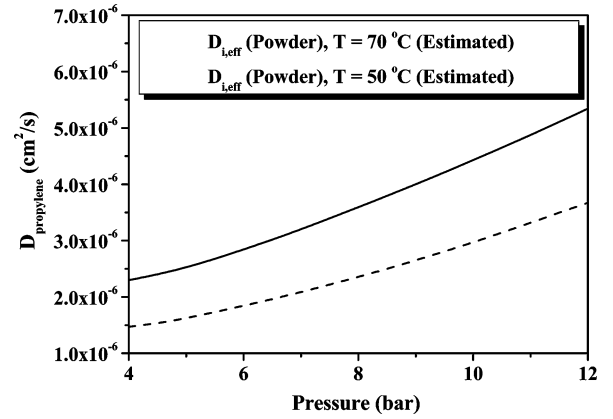

Figure 12. Estimated values of propylene diffusion coefficient, $D_{i,\mathrm{eff}}$, in HDPE powders at different pressures and temperatures.

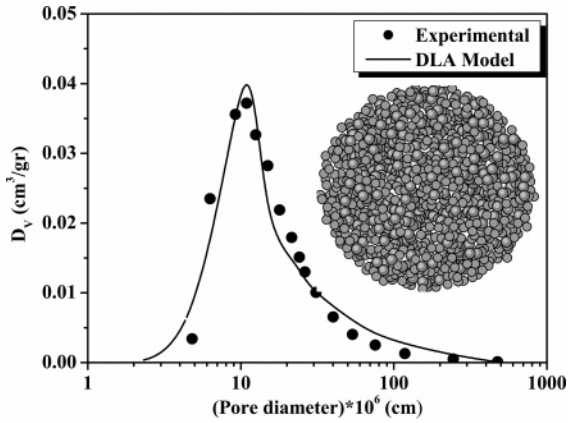

Figure 13. Predicted and measured pore size distributions of Borealis HDPE powder.

Results and Discussion

In Figures 7 and 8, representative ethylene and propylene sorption curves in HDPE films and powders (experimentally measured and shown by the discrete points) are plotted with respect to time at different pressures and temperatures. Continuous lines represent the corresponding theoretical values predicted by the postulated diffusion models (eqs 7−10 and 16−17 and eqs 11−14 and 16−19). Based on the employed diffusion model (i.e., eqs 7−10, 16, and 17) and the corrected dynamic sorption measurements on nonporous polymer films, the numerical value of the pre-exponential constant, $D^{\mathrm{p}}_{0,i}$, in eq 16 was estimated at different temperatures for both ethylene and propylene (see Table 1). It should be pointed out that the estimated values for

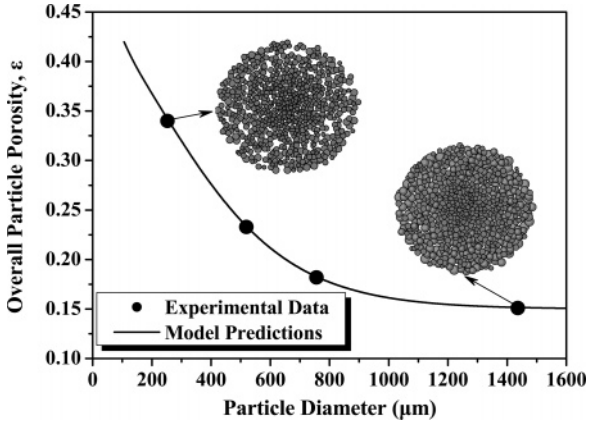

Figure 14. Evolution of particle porosity with respect to particle diameter, at $T = 80$ °C.[44]

Table 2. Numerical Values of the DLA Model Parameters Employed for the Evaluation of the Internal Particle Morphology of HDPE Porous Polymer Particles Supplied by Borealis

parameter	value
number of selected shells in a macroparticle	1
number of formation centers in a shell	4
microparticles diffusion length	1 microparticle radius
total number of diffusing microparticles	125
mean diameter of the log-normal microparticle size distribution (experimental)	64.8 (μm)
standard deviation of the log-normal microparticle size distribution (experimental)	18.5 (μm)
extent of microparticles fusion (calculated in this study)	0.113 (at $T = 50$ °C) 0.132 (at $T = 70$ °C)
overall particle porosity (measured)	0.105

$D^{\mathrm{p}}_{0,i}$ were found to be in good agreement with those reported in the open literature (see Table 1).[38,40−43] In the same table, the numerical values of all the physical and transport parameters used in the theoretical calculations are reported. Subsequently, from the experimental sorption measurements of α-olefins in porous HDPE powders and the estimated values of $D^{\mathrm{p}}_{i,\mathrm{eff}}$ (see eq 17), the porosity of the HDPE porous particles, ϵ, and, thus, the diffusion coefficient $D_{i,\mathrm{eff}}$ of the penetrant molecules were calculated. In the present study, it was found that the porosity for the Borealis HDPE powder was equal to 0.10, which compared fairly well with the experimentally measured value of $\epsilon = 0.105$ obtained via BET sorption/desorption measurements.

In Figures 9−12, the diffusion coefficients $D^{\mathrm{p}}_{i,\mathrm{eff}}$ and $D_{i,\mathrm{eff}}$ of α-olefins in HDPE films and powders, estimated by eqs 17 and 19, respectively, are plotted at different pressures and temperatures. It is evident that the estimated values of the diffusion coefficient, $D_{i,\mathrm{eff}}$, of α-olefins in porous polymer powders, are higher than the corresponding values of the diffusion coefficient, $D^{\mathrm{p}}_{i,\mathrm{eff}}$, in nonporous HDPE films due to the particle porosity, ϵ (see Figures 9−12). Moreover, it was found that the diffusion coefficient increased with temperature, independently of the polymer morphology.

In Figure 13, the pore size distribution of the tested Borealis HDPE powder, obtained from BET sorption/desorption measurements, is depicted (see discrete points). The continuous line represents the pore size distribution calculated by the DLA model. The numerical values of all parameters employed in the DLA model calculations are reported in Table 2. Apparently, there is a very good agreement between experimental measurements and model predictions.

Table 3. Numerical Values of the DLA Model Parameters Employed for the Evaluation of the Internal Particle Morphology of HDPE Polymer Particles[44]

parameter	value			
number of selected shells in a macroparticle	3			
number of formation centers in a shell	4			
microparticle diffusion length	1 microparticle radius			
extent of microparticle fusion (calculated in this study)	0.14 (at $T = 80$ °C)			
overall particle porosity[44]	0.344	0.233	0.182	0.151
total number of diffusing microparticles	820	820	820	820
first shell (center)[44]	(17.4, 4.2)[a]	(30.7, 7.2)	(41.4, 9.1)	(73.5, 15.1)
second shell (middle)[44]	(18.4, 3.9)	(32.9, 6.8)	(43.9, 8.5)	(77.6, 14.6)
third shell (external)[44]	(21.8, 3.6)	(40.0, 6.5)	(52.0, 8.1)	(89.4, 14.1)

[a] Characteristics of the log-normal microparticle size distribution (mean diameter (μm), standard deviation (μm)).

Finally, Figure 14 depicts the time evolution of the overall particle porosity in a Z−N catalytic gas-phase olefin polymerization as measured by Han-Adebekun.[44] It is apparent that as the polymerization proceeds (i.e., the particle diameter increases) the overall particle porosity decreases due to polymer filling of the pores. The two inserted images in Figure 14 illustrate the reconstructed by the DLA model internal particle morphology at two different particle diameters (i.e., polymerization times). The numerical values of all parameters employed in the DLA model calculations were directly obtained from the study of Han-Adebekun and are reported in Table 3.[44]

Conclusions

In the present study, the internal morphology (i.e., porosity, pore size distribution) of polyolefin particles pro duced in catalytic Z−N olefin polymerization reactors was experimentally and theoretically assessed. An unsteady-state diffusion model was first developed to calculate the transport of penetrant molecules in semicrystalline nonporous films and porous polyolefin powders in terms of the internal particle morphology (i.e., pore size distribution and crystallinity) of the polymer. Dynamic sorption experiments of α-olefins (i.e., ethylene, propylene) in nonporous polymer films and porous polyolefin powders were then employed, along with the unsteady-state diffusion model, to evaluate the overall particle porosity. The calculated overall particle porosity, ϵ, of the examined HDPE powder was found to be in very good agreement with the corresponding experimental value of ϵ obtained via BET sorption/desorption measurements. To reconstruct the pore size distribution in a porous polyolefin particle in terms of the estimated overall particle porosity and the size distribution of the microparticles, a DLA model was employed. It was shown that the morphological characteristics of the polyolefin particles (i.e., porosity and pore size distribution) can be modeled in a realistic way, thus, providing the means for calculating the time-dependence of the diffusion coefficient in Z−N catalytic olefin polymerizations.

Acknowledgment

The authors gratefully acknowledge the European Community for supporting this work under the Growth Project G5RD-CT-2001-00597.

Nomenclature

C_i = penetrant's concentration in polymer, kmol/m^3
$C_{i,eq}$ = equilibrium concentration of penetrant i in polymer, kmol/m^3
$D_{i,eff}$ = overall diffusion coefficient of penetrant "i" in the polymer powder, m^2/s
D_i^0 = diffusion coefficient of penetrant "i" in the gas phase, m^2/s
$D_{i.0}^p$ = pre-exponential constant of the diffusion coefficient, m^2/s
$D_{i,eff}^p$ = overall diffusion coefficient of penetrant "i" in polymer phase, m^2/s
F_{ve} = viscoelastic force, Nt
G = Young modulus, kg/(m s^2)
h = center-to-enter distance between collide particles, m
L_k = film length ($k = x,y,z$), m
L_{0k} = initial film length ($k = x,y,z$), m
l_e = strain in the spring, dimensionless
l_v = strain in the dashpot, dimensionless
M_i = penetrant mass uptake, kg
$M_{i,corr}$ = corrected penetrant mass uptake, kg
$M_{i,eq}$ = equilibrium penetrant mass uptake, kg
$M_{i,meas}$ = measured penetrant mass uptake, kg
MW_i = penetrant molecular weight, kg/kmol
P = pressure, Pa
P^* = parameter, Sanchez−Lacombe model, Pa
r = radial position inside the polymer particle, m
r_c = fusion (contact) radius, m
R = particle radius, m
R_0 = initial particle radius, m
t = time, s
T = particle temperature, K
T^* = parameter, Sanchez−Lacombe model, K
T_b = bulk-phase temperature, K
V_i^* = penetrant-specific critical hole free volume, m^3/g
V_p^* = polymer-specific critical hole free volume, m^3/g
V_{pk} = specific critical hole free volume of the polymer jumping unit, m^3/mol
V_{FH} = overall free volume, m^3/g
x = position inside the polymer film, m
x_d = displacement, m
x_i = mole fraction of penetrant i
Y_i = dimensionless penetrant concentration in polymer phase
z = dimensionless position inside the polymer film or powder ($z = (x/L_x(t))$ or $z = (r/R(t))$)

Greek Symbols

γ = overlap factor
γ_s = interfacial tension, Nt/m
ϵ = polymer particle porosity
λ_0 = relaxation time, s
μ = apparent viscosity, kg/(m s)

ξ_{ip} = ratio between the volumes of the diffusing jumping units of the penetrant and the polymer
ρ = density, kg/m^3
ρ_{am} = density of the amorphous polymer phase, kg/m^3
ρ_c = density of the crystalline phase, kg/m^3
ρ^* = parameter, Sanchez Lacombe model, kg/m^3
σ_e = elastic stress, Nt/m^2
σ_i = collision diameter of penetrant molecule i, m
σ_v = viscous stress, Nt/m^2
τ = tortuosity factor used in the random pore model
τ_f = tortuosity factor used in the free volume model
ω_c = degree of crystallinity
ω_i = penetrant mass fraction
ω_p = polymer mass fraction
Ω = collision integral

Literature Cited

(1) Hoel, E. L.; Cozewith, C.; Byrne, G. D. Effect of Diffusion on Heterogeneous Ethylene Propylene Copolymerization. *AIChE J.* **1994**, *40*, 1669.

(2) Hutchinson, R. A.; Chen, C. M.; Ray, W. H. Polymerization of Olefins through Heterogeneous Catalysis X: Modeling of Particle Growth and Morphology. *J. Appl. Polym. Sci.* **1992**, *44*, 1389.

(3) Ferrero, M. A.; Chiovetta, M. G. Effects of Catalyst Fragmentation During Propylene Polymerization. IV: Comparizon Between Gas-Phase and Bulk Polymerization Processes. *Polym. Eng. Sci.* **1991**, *31*, 904.

(4) Soares, J. B. P.; Hamielec, A. E. General Dynamic Mathematical Modelling of Heterogeneous Ziegler-Natta and Metallocene Catalyzed Copolymerization with Multiple Site Types and Mass and Heat Transfer Resistances. *Polym. React. Eng.* **1995**, *3*, 261.

(5) Sun, J.; Eberstein, C.; Reichert, K. H. Particle Growth Modeling of Gas Phase Polymerization of Butadiene. *J. Appl. Polym. Sci*. **1997**, *64* (*2*), 203.

(6) Debling, J. A.; Ray, W. H. Heat and Mass Transfer Effects in Multistage Polymerization Processes: Impact Polypropylene. *Ind. Eng. Chem. Res.* **1995**, *34*, 3466.

(7) Galvan, R.; Tirrell, M. Molecular Weight Distribution Predictions for Heterogeneous Ziegler-Natta Polymerization Using a Two-Site Model. *Chem. Eng. Sci.* **1986**, *41*, 2385.

(8) Hamba, M.; Han-Adebekun, G. C.; Ray, W. H. Kinetic Study of Gas Phase Olefin Polymerization with a $TiCl_4/MgCl_2$ Catalyst. II. Kinetic Parameter Estimation and Model Building. *J. Appl. Polym. Sci. Part A: Polym. Chem.* **1997**, *35*, 2075.

(9) Chiovetta, M. G. Ph.D. Thesis, University of Massachusetts at Amherst, 1983.

(10) Laurence, R. L.; Chiovetta, M. G. Heat and Mass Transfer During Olefin Polymerization From the Gas Phase. In *Polymer Reaction Engineering: Influence of Reaction Engineering on Polymer Properties*; Reichert, K.H., Geisler, W., Eds.; Hanser: Munich, 1983; pp 74−111.

(11) Estenoz, D. A.; Chiovetta, M. G. A Structural Model for the Catalytic Polymerization of Ethylene Using Chromium Catalysts: Part I. Description and Solution. *Polym. Eng. Sci.* **1996**, *36*, 2208.

(12) Estenoz, D. A.; Chiovetta, M. G. A Structural Model for the Catalytic Polymerization of Ethylene Using Chromium Catalysts: Part II. Thermal Effects. *Polym. Eng. Sci.* **1996**, *36*, 2229.

(13) Weist, E. L.; Ali, A. H.; Conner, W. C. Morphological Study of Supported Chromium Polymerization Catalysts. 1. Activation. *Macromolecules* **1987**, *20*, 689.

(14) Weist, E. L.; Ali, A. H.; Naik, B.; Conner, W. C. Morphological Study of Supported Chromium Polymerization Catalysts. 1. Initial Stages of Polymerization. *Macromolecules* **1989**, *22*, 3244.

(15) Galli, P.; Haylock, J. C. Continuing Initiator System Developments Provide a New Horizon for Polyolefin Quality and Properties. *Prog. Polym. Sci.* **1991**, *16*, 443.

(16) Simonazzi, T.; Cecchin, G.; Mazzaullo, S. An Outlook on Progress in Polypropylene-based Polymer Technology. *Prog. Polym. Sci.* **1991**, *16*, 303.

(17) Galli, P. The Reactor Granule Technology: An Original Approach to a Broad Range of Highly Compatible Materials. Presented at the 6th International Workshop on Polymer Reaction Engineering, Dechema Monographs Vol. 134; Wiley-VCH: Berlin, Germany, 1998; pp 61−79.

(18) Galli, P. Challenges in the Reaction Engineering of Polyolefins. Presented at the 1st First European Conference on the Reaction Engineering of Polyolefins, Lyon, France, July 3−6, 2000.

(19) Pater, J. T. M.; Roos, P.; Weickert, G.; Westerterp, K. R.; Shimitzu, F.; Ko, G. Integral Aspects of Gas Phase Olefin Polymerization: Kinetics, Absorption and Fluidization. In *Sixth International Workshop on Polymer Reaction Engineering*; Reichert, K.-H., Moritz, H.-U., Eds.; Dechema Monograph, Vol. 134; Wiley-VCH: Berlin, 1998; pp 103−114.

(20) Agarwal, U. S. Modeling Olefin Polymerization on Heterogeneous Catalyst: Polymer Resistance at the Microparticle Level. *Chem. Eng. Sci.* **1998**, *53*, 3941.

(21) Villadsen, J.; Michelsen, M. L. *Solution of Differential Equation Models by Polynomial Approximation*; Prentice Hall: Englewood Cliffs, NJ, 1978.

(22) Lützow, N.; Tihminlioglu, A.; Danner, R. P.; Duda, J. L.; De Haan, A.; Warnier, G.; Zielinski J. M. Diffusion of Toluene and n-heptane in Polyethylenes of Different Crystallinity. *Polymer* **1999**, *40*, 2797.

(23) Keramopoulos, A.; Kiparissides, C. Mathematical Modeling of Diffusion-controlled Free-radical Terpolymerization Reactions. *J. Appl. Polym. Sci.* **2003**, *88*, 161.

(24) Vrentas, J. S.; Duda, J. L. Diffusion of Small Molecules in Amorphous Polymers. *Macromolecules* **1976**, *9*, 785.

(25) Cussler, E. L. *Diffusion Mass Transfer in Fluid Systems*; University Press: New York, 1997.

(26) Desilets, M.; Proulx, P.; Soucy, G. Modelling of Multicomponent Diffusion in High Temperature Flows. *Int. J. Heat Mass Transfer* **1997**, *40*, 4273.

(27) Benes, N.; Verweij, H. Comparison of Micro- and Microscopic Theories Describing Multicomponent Mass Transport in Microporous Media. *Langmuir* **1999,** *15*, 8292.

(28) Aris, R. *The Mathematical Theory of Diffusion and Reaction in Permeable Catalysts*; Clarendon Press: Oxford, 1975.

(29) Doong, S. J.; Ho, W. S. W. Diffusion of Hydrocarbons in Polyethylene. *Ind. Eng. Chem. Res.* **1992**, *31*, 1050.

(30) Wacao, N.; Smith, J. M. Diffusion and Reaction in Porous Catalysts. *Chem. Eng. Sci.* **1964**, *3*, 321.

(31) Jones, K. W.; Spanne, P.; Lindquist, W. B.; Conner, W. C.; Ferrero, M. Determination of Polymerization Particle Morphology Using Synchroton Computed Microtomography. *Nucl. Instrum. Methods Phys. Res., Sect. B* **1992**, *68*, 105.

(32) Van der Ven, S. *Polypropylene and other Polyolefins: Polymerization and Characterization*; Elsevier Science Publishers B.V.: Amsterdam, 1990.

(33) Mandelbrot, B. B. The Fractal Geometry of Nature; Freeman Co., 1982.

(34) Edwards, S. F.; Schwartz, M. Exact Differential Equations for Diffusion Limited Aggregation. *Physica A* **1996**, *227*, 149.

(35) Kovfics, T.; Bfirdos, G. Cluster Growth by Difffusion-Limited Aggregation in Shear Flow. *Physica A* **1997**, *247*, 59.

(36) Zhi-Jie Tan, Z. J.; Zou, X. W.; Zhang, W. B.; Jin, Z. Z. Influence of External Field on Diffusion-Limited Aggregation. *Phys. Lett. A.* **2000**, *268*, 112.

(37) Bird, R. B.; Armstrong, R. C.; Hassager, O. *Dynamics of Polymeric Liquids. Vol 1. Fluid Mechanics*; Wiley Publishers: New York, 1977.

(38) Kiparissides, C.; Dimos, V.; Boultouka, T.; Anastasiades, A.; Chasiotis, A. An Experimental and Theoretical Investigation of Solubility and Diffusion of Ethylene in Semi-Crystalline PE at Elevated Pressures and Temperatures. *J. Appl. Polym. Sci.* **2003**, *87*, 953.

(39) Kanellopoulos, V.; Mouratides, D.; Pladis, P.; Kiparissides, C. Prediction of Solubility of α-Olefins in Polyolefins Using a Combined Equation of State-Molecular Dynamics Approach. *Ind. Eng. Chem. Res.* **2006**, *45*, 5870.

(40) Pace, R. J.; Datyner, A. Statistical Mechanical Model for Diffusion of Simple Penetrants in Polymers. I. Theory. *J. Polym. Sci. Polym. Phys.* **1979a**, *17*, 437.

(41) Pace, R. J.; Datyner, A. Statistical Mechanical Model of Diffusion of Complex Penetrants in Polymers. I. Theory. *J. Polym. Sci. Polym. Phys.* **1979b**, *17*, 1675.

(42) Van Krevelen, D. W. *Properties of Polymers*; Elsevier Science: Amsterdam, The Netherlands, 1997.

(43) Neogi, P., *Diffusion in Polymers*; Marcel Dekker: New York, 1996.

(44) Han-Adebekun, G. C. Ph.D. Thesis, University of Wisconsin−Madison, 1996.

(45) Brandrup, J.; Immergut, E. H. *Polymer Handbook*; John Wiley & Sons: New York, 1989.

Received for review June 7, 2006
Revised manuscript received December 28, 2006
Accepted January 10, 2007

IE060721S